RESEARCH ARTICLE | SEPTEMBER 01 2023

Interlayer antiferromagnetic coupling in $Tb_3Fe_5O_{12}/Y_3Fe_5O_{12}$ bilayers

Jing Ming Liang ; Xu Wen Zhao ; Xin Yuan ; Yu Kuai Liu ; Sheung Mei Ng ; Hon Fai Wong ; Pei Gen Li ; Yan Zhou ; Fu Xiang Zhang ; Chee Leung Mak ; Chi Wah Leung

Appl. Phys. Lett. 123, 092405 (2023)
https://doi.org/10.1063/5.0157882

Applied Physics Letters
AIP Publishing

Applied Physics Letters ARTICLE pubs.aip.org/aip/apl

Interlayer antiferromagnetic coupling in $Tb_3Fe_5O_{12}/Y_3Fe_5O_{12}$ bilayers

Cite as: Appl. Phys. Lett. **123**, 092405 (2023); doi: 10.1063/5.0157882
Submitted: 12 May 2023 · Accepted: 15 August 2023 ·
Published Online: 1 September 2023

Jing Ming Liang,[1] Xu Wen Zhao,[1] Xin Yuan,[1,2] Yu Kuai Liu,[3] Sheung Mei Ng,[1] Hon Fai Wong,[1] Pei Gen Li,[1] Yan Zhou,[4] Fu Xiang Zhang,[2] Chee Leung Mak,[1] and Chi Wah Leung[1,a)]

AFFILIATIONS

[1]Department of Applied Physics, The Hong Kong Polytechnic University, Hung Hom, Hong Kong, China
[2]Songshan Lake Materials Laboratory, Dongguan, Guangdong 523808, China
[3]College of Electronic Information and Mechatronic Engineering, Zhaoqing University, Zhaoqing, Guangdong 526061, China
[4]School of Science and Engineering, Chinese University of Hong Kong, Shenzhen, Guangdong 518172, China

Note: This paper is part of the APL Special Collection on Ferrimagnetic Spintronics.
[a)]**Author to whom correspondence should be addressed:** dennis.leung@polyu.edu.hk

ABSTRACT

The interlayer antiferromagnetic (AFM) coupling between thin films plays a significant role in the application of spintronics and magnetic memory devices. Previously, we observed AFM coupling phenomenon at low temperatures in rare-earth iron garnet bilayers epitaxially grown on $Y_3Al_5O_{12}$ substrates. Here, we report a detailed study on the impacts of various factors, including temperature, crystallographic orientation, and layer thickness, on the AMF coupling and magnetization reversal behavior of such a bilayer system. A simple energy model qualitatively described the coupling behavior of the two layers during the magnetization reversal process. The interlayer coupling strength was calculated by measuring the minor magnetic hysteresis loops. The current results can serve as a reminder for future research on interlayer AFM coupling phenomena and highlight the potential of manipulating the magnetic properties in rare-earth garnet bilayers for spintronics studies and other applications.

Yttrium iron garnet ($Y_3Fe_5O_{12}$, YIG) is an extensively studied ferrimagnetic insulator with low Gilbert damping constant[1] and long spin-wave propagation lifetime,[2] which make it an important candidate for various spintronics devices. For example, YIG/heavy metal interfaces are reported to demonstrate spin transport behavior, such as spin pumping,[3] spin Hall magnetoresistance,[4] spin Seebeck effect,[5] and many others.[6]

In various spintronics applications, the engineering of interfacial magnetic coupling allows us to enhance functionalities. A notable example is the antiferromagnetic (AFM) coupling, which can be used for manipulating the magnetic configurations and magnetization reversal processes.[7] In some cases, AFM coupling can lead to a negative remanent magnetization, manifested with an inverted magnetic hysteresis loop (IHL).[8–10] For a normal magnetic hysteresis (M–H) loop, a negative external field is needed to bring the magnetization to zero (assuming that it is saturated with a positive field at the beginning), while for IHL the magnetization reduces to zero during the demagnetization process when the field is still positive.[8]

Iron garnet-based multilayers have recently attracted attention for the studies of magnon valves,[11] and it is legitimate to question about the possibility of magnetic coupling among such structures. To date, the most studied iron garnet-based multilayer systems are YIG/ferromagnetic metal bilayers, such as YIG/Permalloy[12] and YIG/Co,[13] but the magnetic coupling between YIG and other rare-earth iron garnets (REIG) remains to be explored. There are recent reports[14] demonstrating that YIG epitaxially grown on $Gd_3Ga_5O_{12}$ (GGG) substrates can present an AFM coupling, due to the growth-induced $Gd_3Fe_5O_{12}$ (GdIG) layer at the film/substrate interface. Similarly, AFM coupling was observed in $Tb_3Fe_5O_{12}$ (TbIG)/YIG bilayers at low temperatures in our previous study.[15]

For IHL phenomenon, it has been observed in either particles[16] and thin films forms.[17] Most of these IHL-related reports are based on metallic ferromagnetic films,[8,9,17,18] and reports involving oxides insulators are limited. Furthermore, there is a lack of research in exploring the influencing factors for AFM coupling effect on garnet bilayers.

In this report, we conduct an in-depth study of the factors that influence the interlayer AFM coupling in TbIG/YIG bilayers deposited

on $Y_3Al_5O_{12}$ (YAG) substrates, based on preliminary observations in our previous study.[15] A simple model is constructed to provide a qualitative depiction of how the individual garnet layers respond upon the presence of interlayer AFM coupling. Concurrently, the effects of various factors on the strength of the interlayer coupling (J_{AF}) are evaluated utilizing the measurement of minor M–H loops. AFM coupling between YIG and TbIG is detected at low temperatures of 10 K, and this manifests as an IHL phenomenon when there is an appropriate combination of layer thicknesses. The strength of the AFM coupling is highly dependent on temperature. Furthermore, the crystallographic orientations also have a significant influence, with samples deposited on (100)-oriented substrates exhibiting a stronger AFM coupling strength.

Epitaxial TbIG(d_{TbIG})/YIG (d_{YIG}) (where d_{TbIG} and d_{YIG} refer to the thickness of the corresponding layers in nanometers) were deposited on YAG single crystal substrates by pulsed laser deposition (PLD). Detailed film deposition conditions and characterization methods can be found in Ref. 15. The temperature dependence of magnetization was studied on TbIG (7)/YIG (23)/YAG (100) samples. The crystallographic orientation effect was studied on TbIG (7)/YIG (23) bilayers deposited on YAG substrates with (100), (110), and (111) orientations. Finally, the thickness effect was studied on TbIG (d_{TbIG})/YIG (23) bilayers ($d_{TbIG} = 4$, 7, 10, or 15 nm) on (110)-orientated YAG substrates.

Figure 1(a) presents the XRD pattern of TbIG (7)/YIG (23) bilayer on YAG (100) substrate. Only one main peak of the bilayer film alongside the (400) peak of the substrate can be identified. The peaks of YIG and TbIG are merged into one main peak due to the similar lattice constants of YIG and TbIG and the small thickness of the TbIG layer. The strong oscillation near the main peak indicates the excellent quality of the sample.

The corresponding high-angle annular-dark-field (HAADF) scanning transmission electron microscopy (STEM) cross section images of the bilayer sample are displayed in Figs. 1(b)–1(d). Figure 1(b) illustrates the high uniformity of the bilayer sample with no observable defects. Sharp interfaces between TbIG/YIG and YIG/YAG are identified, and the thickness of each layer is close to our design. The STEM images of the interfaces of TbIG/YIG and YIG/YAG with atomic resolution are shown in Figs. 1(c) and 1(d), respectively, confirming the excellent epitaxial growth of the bilayer. The energy-dispersive x-ray spectroscopy (EDX) profile in Fig. 1(e) was used to probe the element diffusion, with an ~2 nm of interdiffusion length, no obvious interdiffusion between layers is observed, and this result is similar to other reports.[19]

Figure 2(a) shows the M–H loops at 10 K of TbIG (7)/YIG (23) bilayer on YAG (100) substrate, with in-plane magnetic field (H) applied along the [001] direction. The loop shows double coercivity due to the difference of anisotropy constant between TbIG ($K_{TbIG} \approx -7.98 \times 10^4$ J/m^3) and YIG ($K_{YIG} \approx -2.48 \times 10^3$ J/m^3).[20] Notably, IHL phenomenon can be clearly identified. With increasing temperature, the double coercivity phenomenon gradually weakens and disappears at around 80 K. The IHL returns to the normal state when the temperature is higher than 70 K [Fig. 2(b)].

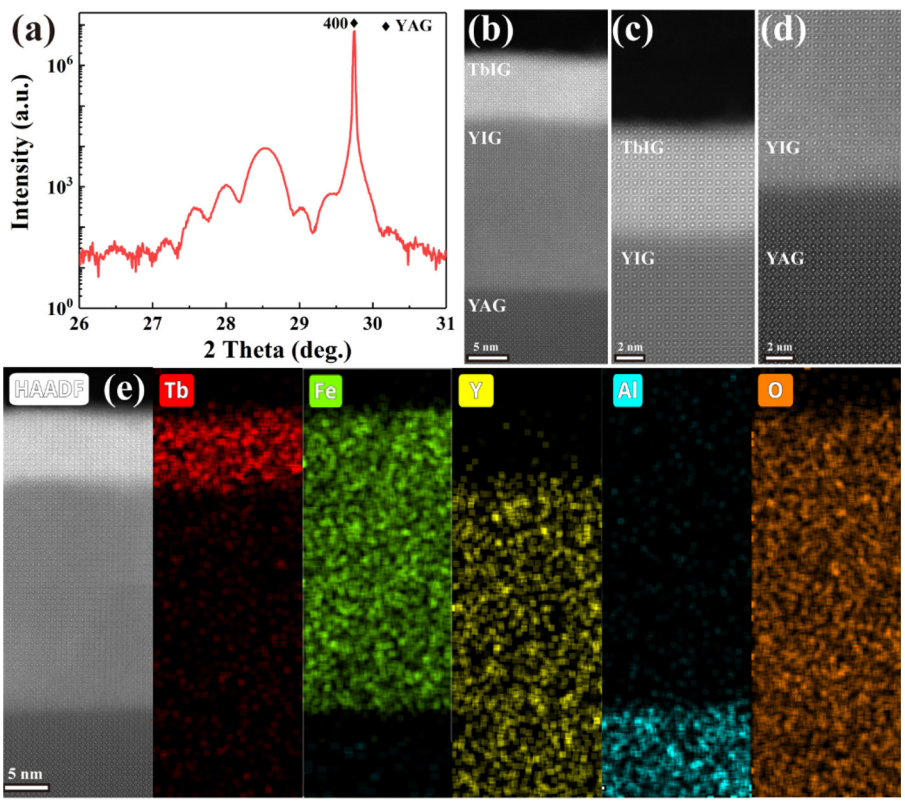

FIG. 1. (a) XRD 2θ scan of TbIG (7)/YIG (23) bilayer on YAG (100) substrate. (b) Corresponding cross-sectional HAADF-STEM image. Interface images of TbIG/YIG (c) and YIG/YAG (d) with high magnification. (e) EDX mapping of Tb, Fe, Y, Al, and O.

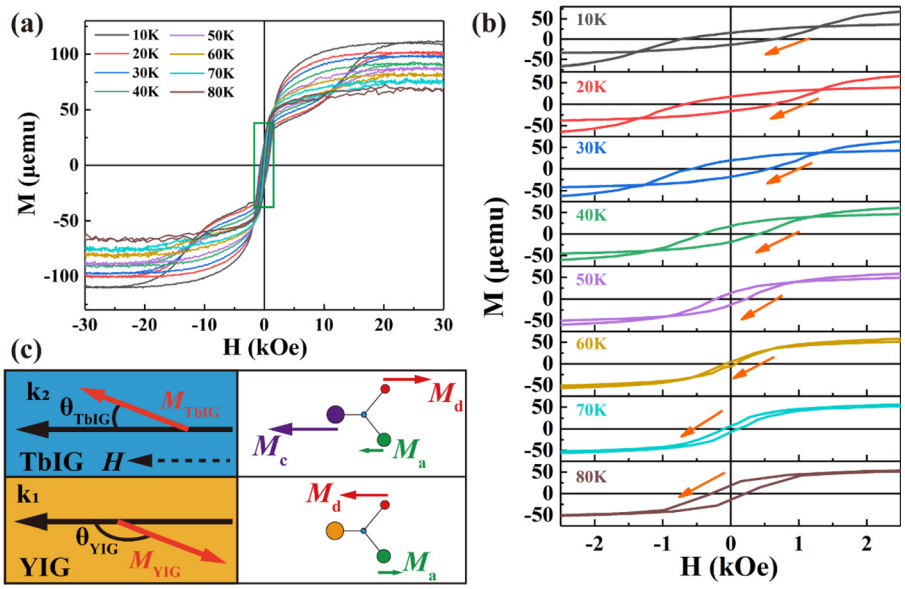

FIG. 2. (a) In-plane M–H loops of TbIG (7)/YIG (23) bilayer on YAG (100) substrate at different temperatures, with the magnified view of the low-field region shown in (b). The field sweeping directions are indicated by arrows. (c) The magnetic schematic model of the bilayer system, with the symbols defined in the text.

A schematic diagram in Fig. 2(c) further illustrates the AFM-coupled TbIG/YIG bilayer system. YIG has *A*-site (octahedral-sites) Fe^{3+} (M_a) and *D*-site (tetrahedral-sites) Fe^{3+} (M_d) ions arranged in an anti-parallel manner, with the net magnetization dominated by the *D*-site Fe^{3+}.[21] Compared with YIG, TbIG has additional magnetization contribution from the *C*-site (dodecahedral-sites) Tb^{3+} (M_c) ions, which dominate the overall magnetization of TbIG at low temperatures.[22] As mentioned before, the drastic difference between K_{TbIG} and K_{YIG} results in the non-synchronous rotation of YIG (M_{YIG}) and TbIG (M_{TbIG}) magnetizations. When H is reduced from positive saturation, the YIG layer first reverses before H reaches zero, while the TbIG layer remains unchanged. In the absence of coupling between two magnetic layers, one should expect the YIG to be switched only after H turns negative. To explain the YIG reversal at a positive external field upon decreasing H (i.e., a positive coercive field), as well as the IHL, AFM coupling is invoked as discussed in the following.

The AFM coupling between YIG and TbIG can be represented with a coupling constant J_{AF}, and the total energy (per unit area) of the bilayer system (based on Stoner–Wohlfarth model) can be expressed as follows:[23]

$$\begin{aligned} E = {} & K_{YIG} d_{YIG} \sin^2\theta_{YIG} + K_{TbIG} d_{TbIG} \sin^2\theta_{TbIG} \\ & - M_{YIG} d_{YIG} H \cos(\theta_{YIG} - \theta_H) \\ & - M_{TbIG} d_{TbIG} H \cos(\theta_{TbIG} - \theta_H) - J_{AF} \cos(\theta_{YIG} - \theta_{TbIG}). \end{aligned} \quad (1)$$

In Eq. (1), K corresponds to the anisotropy constant, d is the layer thickness, θ is the angle between the magnetization M and the easy axis of the layer, and θ_H is the angle of the applied magnetic field. The anisotropy energies of each layer are expressed in the first two terms of Eq. (1), followed by the Zeeman energy in each layer. The last term corresponds to the magnetic coupling between the two layers. At the minimum energy state of the bilayer system, $\delta E/\delta\theta_{YIG} = \delta E/\delta\theta_{TbIG} = 0$. Therefore, four solutions can be obtained [Fig. 3(a)]: (i) $\theta_{YIG} = \theta_{TbIG} = 0$, (ii) $\theta_{YIG} = \pi$, $\theta_{TbIG} = 0$, (iii) $\theta_{YIG} = 0$, $\theta_{TbIG} = \pi$, and (iv) $\theta_{YIG} = \theta_{TbIG} = \pi$.

Through Eq. (1), the IHL phenomenon of the TbIG/YIG bilayer system can be described as follows. First, state (i) is the most stable situation with large and positive H, at which M_{YIG} and M_{TbIG} both point along H. When H is gradually reduced, the stable state becomes either state (ii) or (iii), depending on the energy associated with the magnetic configurations. Considering K_{TbIG} greater than K_{YIG}, M_{YIG} is reversed at H_{c1}, where H_{c1} is a critical field at which the increased Zeeman energy compensates for the reduced AFM coupling energy due to the reversal of YIG layer. A reversal at positive H can, therefore, be observed. As the overall magnetization of the YIG layer is larger than that of the TbIG layer, IHL can be observed. Subsequently, when H arrives at H_{c2}, the magnetization of TbIG flips from state (ii) to state (iv).

To further verify the AFM coupling effect, Fig. 3(b) shows the minor loops measurements at 10 K of TbIG (7)/YIG (23) bilayer on YAG (100). The magnetic field is swept from either positive (+30 kOe) and negative (−30 kOe) saturation and returning to the starting field at some intermediate fields (−3 and +3 kOe, respectively) of opposite polarities. As demonstrated in Fig. 3(b), a horizontal shift (H_{ex}, ≈1300 Oe) of the YIG loop reminiscent of an exchange bias field is observed, which is consistent with the schematic model in Fig. 3(a), and the shift of the YIG loop also testifies the presence of AFM coupling. Therefore, J_{AF} can be calculated according to the following equation:[24,25]

$$J_{AF} = H_{ex} d_{YIG} M_{YIG}. \quad (2)$$

The minor loops measured from 20 to 80 K can refer to the supplementary material (Fig. S2). The calculated J_{AF} value at 10 K is about −0.57 mJ/m^2, which is comparable with other report (−0.16 mJ/m^2 in the Co/Cu/Co system and −0.6 mJ/m^2 in the Fe/Mn/Fe system).[25,26] With increasing temperatures to 80 K, J_{AF} gradually decreases to about −0.059 mJ/m^2 as evidenced from the decrease in corresponding H_{ex} of YIG loops.

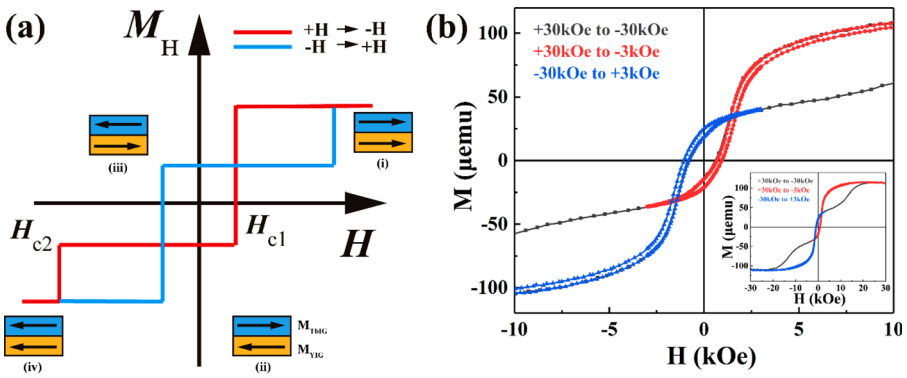

FIG. 3. (a) Schematic M–H loop of TbIG/YIG bilayer based on the model of Fig. 2(c). Symbols are defined in the text. (b) Enlarged minor loops of the TbIG (7)/YIG (23) bilayer on YAG (100), overlaying on the complete M–H loop. The inset shows the loops in the full field range (±30 kOe). All loops are measured at 10 K.

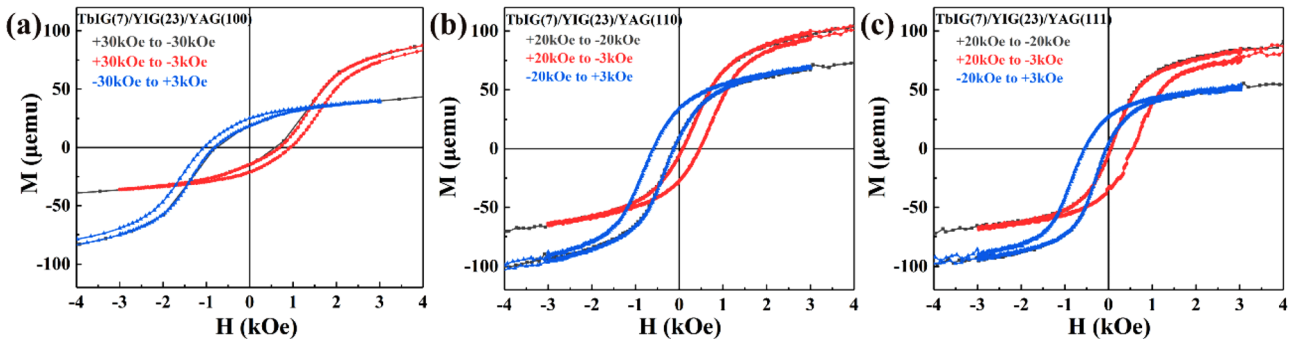

FIG. 4. Enlarged M–H minor loops at 10 K of TbIG (7)/YIG (23) samples on (a) YAG (100) substrate, (b) YAG (110) substrate, and (c) YAG (111) substrate.

TbIG thin films grown on substrates with different orientations can acquire different anisotropy values.[27] Here, we attempt to establish the link between crystallographic orientation and the AFM coupling (Fig. 4). Figures 4(a)–4(c) show the enlarged in-plane M–H minor loops at 10 K of TbIG (7)/YIG (23) bilayers on YAG substrate with (100), (110), and (111) orientations, respectively. When the magnetic field decreases from a large enough positive value to −3 kOe, the YIG layer finishes its reversal [i.e., stage (ii) of Fig. 3(a)]. Thus, the AFM coupling effect as well as the IHL phenomenon can be observed for all samples. However, the H_{ex} shows a great difference for samples grown on different substrates, as H_{ex} of the (100)-orientated bilayer is much stronger compared with the nearly identical H_{ex} values in (110) and (111)-orientated samples. The calculated J_{AF} values of TbIG (7)/YIG (23) bilayers with different crystallographic orientations are different. Among the samples, $J_{AF\text{-}(100)}$ presents the largest value (−0.57 mJ/m^2) at 10 K, while $J_{AF\text{-}(110)}$ and $J_{AF\text{-}(111)}$ are about −0.21 and −0.17 mJ/m^2, respectively.

To investigate the TbIG thickness effect, four bilayer samples of TbIG (d)/YIG (23) (d = 4, 7, 10, and 15 nm) were deposited on YAG (110) substrates. XRD 2θ scans of these samples (Fig. S3) show a shift of YIG/TbIG peak to lower angles when TbIG layer thickness increases, indicating the gradually increased signal from TbIG layer. Both of YIG and TbIG peaks are on the left-side of YAG (110) due to the in-plane compressive strain presented in the bilayer samples.

Figure 5(a) shows the in-plane M–H loops at 10 K of the bilayers. The M_s of the samples, as well as double coercivity phenomenon, are enhanced by the increase in the TbIG layer thickness. Figure 5(b) is the enlarged low field region marked in Fig. 5(a). With increasing TbIG thickness, the M–H loop first shifts to the inverted state and then back to the normal state, indicating the layer thickness has a strong influence on the interlayer AFM coupling behavior.[28] Detailed minor loops of these four samples are illustrated in Fig. 6.

For TbIG (4)/YIG (23) bilayer [Fig. 6(a)], H_{ex} is about 90 Oe and the corresponding calculated J_{AF} is only about −0.04 mJ/m^2. The M_s of bilayer is dominated by the YIG layer and appears like a normal M–H loop. When d_{TbIG} increases to about 7 nm [Fig. 6(b)], H_{ex} increase to about 470 Oe and the J_{AF} is around −0.21 mJ/m^2. However, with

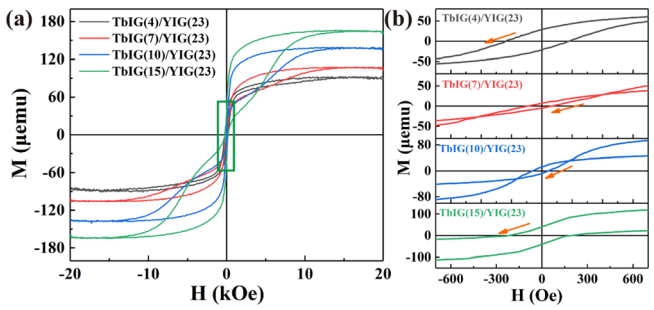

FIG. 5. (a) In-plane M–H loops of TbIG(d)/YIG (23) samples (d = 4, 7, 10, and 15 nm) at 10 K. (b) Highlighted low fields regions of the M–H loops.

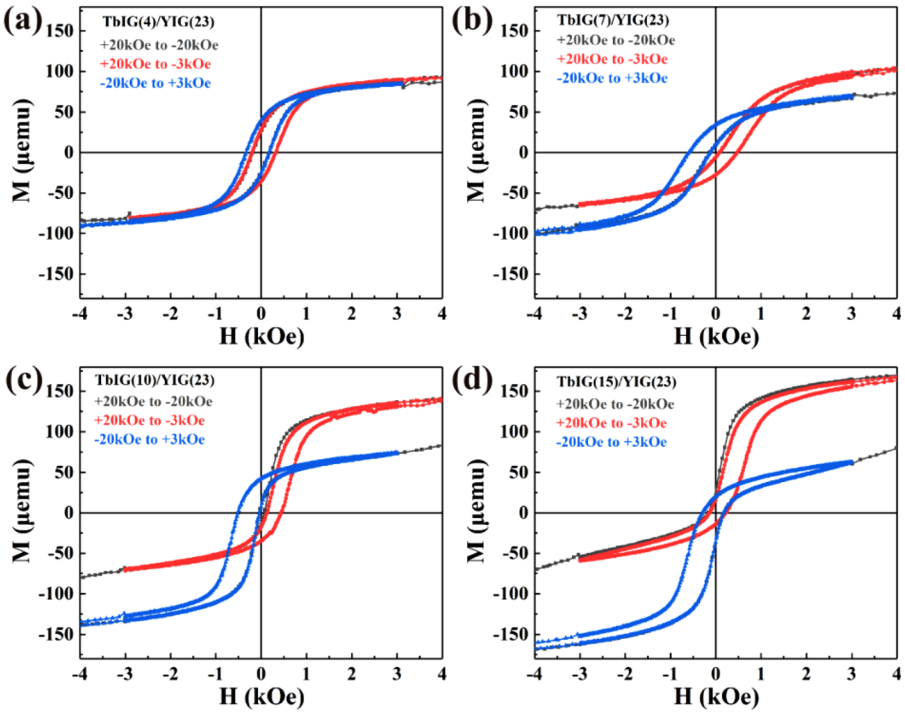

FIG. 6. (a)–(d) Enlarged M–H minor loops at 10 K of TbIG (*d*)/YIG (23) bilayers ($d = 4$, 7, 10, and 15 nm) on YAG (110) substrates.

continue increase in d_{TbIG}, H_{ex} and J_{AF} begin to decrease to about 440 Oe and −0.19 mJ/m^2, respectively [Fig. 6(c)]. For TbIG (15)/YIG (23) bilayer, the H_{ex} and J_{AF} continue decrease to about 380 Oe and −0.16 mJ/m^2, respectively [Fig. 6(d)].

In the current study, the AFM coupling in TbIG/YIG bilayers was systematically studied, and a simple model was established to illustrate such coupling during demagnetization process. Non-synchronous reversal of magnetization can be observed in form of double coercivity phenomenon, thanks to the large difference of anisotropy in TbIG and YIG.[29] In addition, when the M_s values of the two layers differ greatly, the IHL phenomenon can be induced under certain conditions (such as low temperature or certain film thickness combinations).[23,30] The strength of AFM coupling can be influenced by temperature, crystallographic orientation, and film thickness.

In summary, our study explored the AFM coupling of TbIG/YIG bilayer systems as well as the corresponding influencing factors. The AFM coupling strength of the bilayers were calculated by extracting the H_{ex} from minor M–H loops. The temperature, crystallographic orientation, and film thickness showed obvious effect on the coupling strength. The findings provide different strategies for modifying the interlayer coupling of rare-earth garnet bilayer systems, which are particularly relevant to the research on antiferromagnetic spintronic devices.

See the supplementary material for microstructural and epitaxial characterization of TbIG (7)/YIG (23) bilayer sample and the corresponding minor loops measured from 20 to 80 K.

This work was supported by the Hong Kong Research Grants Council (Grant No. 15302320), the Hong Kong Polytechnic University (ZVWC, No. CD6U), the Research Fund of Zhaoqing University (No. 2021011832), and the Guangdong Special Support Project (No. 2019BT02X030).

AUTHOR DECLARATIONS

Conflict of Interest

The authors have no conflicts to disclose.

Author Contributions

Jing Ming Liang: Conceptualization (lead); Data curation (lead); Investigation (lead); Methodology (lead); Validation (lead); Writing – original draft (lead). **Chee Leung MAK:** Funding acquisition (equal); Validation (supporting). **Chi Wah Leung:** Funding acquisition (lead); Project administration (lead); Supervision (lead); Validation (lead); Writing – review & editing (lead). **Xu Wen Zhao:** Methodology (supporting); Validation (supporting); Writing – review & editing (supporting). **Xin Yuan:** Data curation (supporting); Methodology (supporting). **Yu Kuai Liu:** Funding acquisition (equal); Validation (supporting); Writing – review & editing (supporting). **Sheung Mei Ng:** Methodology (supporting); Validation (supporting); Writing – review & editing (supporting). **Hon Fai Wong:** Data curation (supporting); Methodology (supporting); Validation (supporting). **Pei Gen Li:** Methodology (supporting); Validation (supporting). **Yan Zhou:** Funding acquisition (equal); Validation (supporting). **Fuxiang Zhang:** Data curation (supporting); Methodology (supporting); Resources (supporting).

DATA AVAILABILITY

The data that support the findings of this study are available from the corresponding author upon reasonable request.

REFERENCES

[1]G. Schmidt, C. Hauser, P. Trempler, M. Paleschke, and E. T. Papaioannou, Phys. Status Solidi B **257**(7), 1900644 (2020).
[2]L. J. Cornelissen, J. Liu, R. A. Duine, J. Ben Youssef, and B. J. van Wees, Nat. Phys. **11**(12), 1022 (2015).
[3]Y. Kajiwara, K. Harii, S. Takahashi, J. Ohe, K. Uchida, M. Mizuguchi, H. Umezawa, H. Kawai, K. Ando, K. Takanashi, S. Maekawa, and E. Saitoh, Nature **464**(7286), 262 (2010); E. Saitoh, M. Ueda, H. Miyajima, and G. Tatara, Appl. Phys. Lett. **88**(18), 182509 (2006).
[4]N. Vlietstra, J. Shan, V. Castel, B. J. van Wees, and J. Ben Youssef, Phys. Rev. B **87**(18), 184421 (2013); H. Nakayama, M. Althammer, Y. T. Chen, K. Uchida, Y. Kajiwara, D. Kikuchi, T. Ohtani, S. Geprags, M. Opel, S. Takahashi, R. Gross, G. E. Bauer, S. T. Goennenwein, and E. Saitoh, Phys. Rev. Lett. **110**(20), 206601 (2013).
[5]D. Qu, S. Y. Huang, J. Hu, R. Wu, and C. L. Chien, Phys. Rev. Lett. **110**(6), 067206 (2013).
[6]Y. B. Fan, P. Quarterman, J. Finley, J. H. Han, P. Zhang, J. T. Hou, M. D. Stiles, A. J. Grutter, and L. Q. Liu, Phys. Rev. Appl. **13**(6), 061002 (2020); Y. Xiong, Y. Li, M. Hammami, R. Bidthanapally, J. Sklenar, X. Zhang, H. Qu, G. Srinivasan, J. Pearson, A. Hoffmann, V. Novosad, and W. Zhang, Sci. Rep. **10**(1), 12548 (2020).
[7]M. J. Meijer, J. Lucassen, O. Kurnosikov, H. J. M. Swagten, B. Koopmans, R. Lavrijsen, F. Kloodt-Twesten, R. Fromter, and R. A. Duine, Phys. Rev. Lett. **124**(20), 207203 (2020); K. Wang, L. J. Qian, S. C. Ying, and G. Xiao, Phys. Rev. B **102**(14), 144430 (2020).
[8]K. Takanashi, H. Kurokawa, and H. Fujimori, Appl. Phys. Lett. **63**(11), 1585 (1993).
[9]M. J. O'Shea and A. L. Al-Sharif, J. Appl. Phys. **75**(10), 6673 (1994).
[10]H. Zhang, J. Zhang, J. E. Zhang, F. R. Han, H. L. Huang, J. H. Song, B. G. Shen, and J. R. Sun, Chin. Phys. B **28**(3), 037501 (2019).
[11]H. Wu, L. Huang, C. Fang, B. S. Yang, C. H. Wan, G. Q. Yu, J. F. Feng, H. X. Wei, and X. F. Han, Phys. Rev. Lett. **120**(9), 097205 (2018); J. Cramer, F. Fuhrmann, U. Ritzmann, V. Gall, T. Niizeki, R. Ramos, Z. Qiu, D. Hou, T. Kikkawa, J. Sinova, U. Nowak, E. Saitoh, and M. Klaui, Nat. Commun. **9**(1), 1089 (2018).
[12]P. Quarterman, Y. B. Fan, Z. J. Chen, C. J. Jensen, R. V. Chopdekar, D. A. Gilbert, M. E. Holtz, M. D. Stiles, J. A. Borchers, K. Liu, L. Q. Liu, and A. J. Grutter, Phys. Rev. Mater. **6**(9), 094418 (2022).
[13]S. Klingler, V. Amin, S. Geprags, K. Ganzhorn, H. Maier-Flaig, M. Althammer, H. Huebl, R. Gross, R. D. McMichael, M. D. Stiles, S. T. B. Goennenwein, and M. Weiler, Phys. Rev. Lett. **120**(12), 127201 (2018).
[14]M. J. Roos, P. Quarterman, Jinjun Ding, Mingzhong Wu, B. J. Kirby, and B. L. Zink, Phys. Rev. Mater. **6**(3), 034401 (2022); R. Kumar, S. N. Sarangi, D. Samal, and Z. Hossain, Phys. Rev. B **103**(6), 064421 (2021); J. M. Gomez-Perez, S. Velez, L. McKenzie-Sell, M. Amado, J. Herrero-Martin, J. Lopez-Lopez, S. Blanco-Canosa, L. E. Hueso, A. Chuvilin, J. W. A. Robinson, and F. Casanova, Phys. Rev. Appl. **10**(4), 044046 (2018).
[15]J. M. Liang, X. W. Zhao, S. M. Ng, H. F. Wong, Y. K. Liu, C. L. Mak, and C. W. Leung, IEEE Trans. Magn. **58**(2), 2200205 (2022).
[16]R. K. Zheng, H. Liu, Y. Wang, and X. X. Zhang, J. Appl. Phys. **96**(9), 5370 (2004); J. Geshev, A. D. C. Viegas, and J. E. Schmidt, *ibid.* **84**(3), 1488 (1998); Y. J. Nam and S. H. Lim, Appl. Phys. Lett. **99**(9), 092503 (2011).
[17]C. Gao and M. J. O'Shea, J. Magn. Magn. Mater. **127**(1–2), 181 (1993); D. Kim, C. Kim, C. O. Kim, S. S. Yoon, M. Naka, M. Tsunoda, and M. Takahashi, J. Magn. Magn. Mater. **304**(1), E356 (2006).
[18]S. Demirtas, M. R. Hossu, M. Arikan, A. R. Koymen, and M. B. Salamon, Phys. Rev. B **76**(21), 214430 (2007); S. M. Valvidares, L. M. Álvarez-Prado, J. I. Martín, and J. M. Alameda, Phys. Rev. B **64**(13), 134423 (2001).
[19]A. Mitra, O. Cespedes, Q. Ramasse, M. Ali, S. Marmion, M. Ward, R. M. D. Brydson, C. J. Kinane, J. F. K. Cooper, S. Langridge, and B. J. Hickey, Sci. Rep. **7**(1), 11774 (2017); H. C. Chang, T. Liu, D. R. Hickey, P. A. P. Janantha, K. A. Mkhoyan, and M. Z. Wu, APL Mater. **5**(12), 126104 (2017); J. C. Gallagher, A. S. Yang, J. T. Brangham, B. D. Esser, S. P. White, M. R. Page, K. Y. Meng, S. S. Yu, R. Adur, W. Ruane, S. R. Dunsiger, D. W. McComb, F. Y. Yang, and P. C. Hammel, Appl. Phys. Lett. **109**(7), 072401 (2016).
[20]P. Hansen, J. Appl. Phys. **45**(8), 3638 (1974).
[21]T. Yamagishi, J. Awaka, Y. Kawashima, M. Uemura, S. Ebisu, S. Chikazawa, and S. Nagata, Philos. Mag. **85**(17), 1819 (2005).
[22]S. Geller, J. P. Remeika, R. C. Sherwood, H. J. Williams, and G. P. Espinosa, Phys. Rev. **137**(3A), A1034 (1965).
[23]Y. Z. Wu, G. S. Dong, and X. F. Jin, Phys. Rev. B **64**(21), 214406 (2001).
[24]Y. Liu, J. G. Yu, and H. C. Zhong, J. Magn. Magn. Mater. **473**, 381 (2019).
[25]Z. Q. Qiu, J. Pearson, and S. D. Bader, Phys. Rev. B **46**(13), 8659 (1992).
[26]S. T. Purcell, M. T. Johnson, N. W. McGee, R. Coehoorn, and W. Hoving, Phys. Rev. B **45**(22), 13064 (1992).
[27]R. F. Pearson, J. Appl. Phys. **33**(3), 1236 (1962).
[28]P. J. Bloemen, M. T. Johnson, M. T. van de Vorst, R. Coehoorn, J. J. de Vries, R. Jungblut, J. aan de Stegge, A. Reinders, and W. J. de Jonge, Phys. Rev. Lett. **72**(5), 764 (1994).
[29]A. López-Ortega, M. Estrader, G. Salazar-Alvarez, A. G. Roca, and J. Nogués, Phys. Rep. **553**, 1 (2015); M. Estrader, A. Lopez-Ortega, S. Estrade, I. V. Golosovsky, G. Salazar-Alvarez, M. Vasilakaki, K. N. Trohidou, M. Varela, D. C. Stanley, M. Sinko, M. J. Pechan, D. J. Keavney, F. Peiro, S. Surinach, M. D. Baro, and J. Nogues, Nat. Commun. **4**, 2960 (2013); F. Casoli, F. Albertini, L. Nasi, S. Fabbrici, R. Cabassi, F. Bolzoni, and C. Bocchi, Appl. Phys. Lett. **92**(14), 142506 (2008); A. J. Zambano, H. Oguchi, I. Takeuchi, Y. Choi, J. S. Jiang, J. P. Liu, S. E. Lofland, D. Josell, and L. A. Bendersky, Phys. Rev. B **75**(14), 144429 (2007).
[30]T. Kobayashi, H. Tsuji, S. Tsunashima, and S. Uchiyama, Jpn. J. Appl. Phys., Part 2 **20**(11), 2089 (1981).